Correlation of Crack-Tip Opening Angle for Stable Crack Propagation with Charpy and Drop-Weight Tear Test Properties in High-Toughness API X70 Pipeline Steels

BYOUNGCHUL HWANG, SANG YONG SHIN, SUNGHAK LEE, NACK J. KIM, SANGHO KIM, and KI BONG KANG

Correlation between Charpy V-notch (CVN) impact properties, drop-weight tear test (DWTT) properties, and crack-tip opening angles for stable crack propagation ($CTOA_{sc}$) in high-toughness API X70 pipeline steels was investigated in this study. Two-specimen CTOA test (TSCT) was conducted on the rolled steel materials to measure the $CTOA_{sc}$, and the test results were compared to the CVN and DWTT data to find correlations between them. The CVN total energy density showed an almost 1:1 linear correlation with the DWTT initiation energy density. The TSCT results indicated that the materials rolled in the single-phase region had the larger $CTOA_{sc}$ as well as the higher CVN and DWTT energy density than those rolled in the two-phase region because their microstructures were composed of acicular ferrites and fine polygonal ferrites. The $CTOA_{sc}$ had a better correlation with the DWTT propagation energy density or the CVN total energy density than the DWTT total energy density. In particular, the value of sin ($2CTOA_{sc}$) reliably represented a linear proportional relation to the DWTT propagation energy density.

I. INTRODUCTION

CURRENT models for characterizing arrest toughness of dynamic ductile fracture in gas-transmission pipelines have used upper shelf energy (USE) of Charpy V-notch (CVN) impact test and USE of drop-weight tear test (DWTT) as fracture resistance values.[1] In general, the arrest toughness of pipeline steels is predicted by a simplified semiempirical formula obtained from the correlation of fracture speed of pipelines with crack propagation speed, which depends on gas decompression behavior. According to the API RP 5L3 specification,[2] the CVN USE shows a linear relation with the USE of the pressed-notch (PN) DWTT or the chevron-notch (CN) DWTT. In the case of the currently produced high-toughness pipeline steels, however, the correlation of the CVN USE with fundamental fracture process or crack speed is less obvious. This is because a considerable amount of initiation energy is involved, which is unrelated to actual material resistance to fracture propagation as plastic deformation significantly increases at the crack tip.[3,4,5] Also, the impact testing methods are limited by specimen geometries, and the reliability of the correlation between CVN USE and DWTT USE decreases. The evaluation of the absorbed energy has provided reliable standards for low-toughness pipeline steels (CVN USE $\leq$ 100 J), but it is more or less inconsistent with full-scale fracture behavior in currently produced high-toughness pipeline steels.

BYOUNGCHUL HWANG, Postdoctoral Research Associate, and SANG YONG SHIN, Research Assistant, are with the Center for Advanced Aerospace Materials, Pohang University of Science and Technology, Pohang, 790-784 Korea. SUNGHAK LEE and NACK J. KIM, Professors, Center for Advanced Aerospace Materials, Pohang University of Science and Technology, are jointly appointed with the Materials Science and Engineering Department, Pohang University of Science and Technology. Contact e-mail: shlee@postech.ac.kr SANGHO KIM, Principal Researcher, and KI BONG KANG, Group Leader, are with the Plate Research Group, Technical Research Laboratories, POSCO, Pohang 790-785, Korea.

Manuscript submitted December 9, 2004.

Since the 1980s, many investigators have persistently endeavored to specify material resistance to fracture propagation using fracture mechanics variables such as crack-tip stress or strain, crack-tip opening displacement (CTOD) or crack-tip opening angle (CTOA), crack-tip force, energy release rate, J-integral, and tearing modulus.[6–9] Among them, the CTOA at a specified distance from a crack tip, *i.e.*, the CTOA for stable crack propagation ($CTOA_{sc}$), has been shown to be the most appropriate variable for modeling the stable crack growth and instability during the fracture process of pipeline steels. It has been used in aerospace industrial fields to predict the initiation of stable crack growth and was reported to remain constant irrespective of crack extension occurring during the steady-state fracture process.[10] The application of the CTOA to pipeline industries was extensively started in the late 1980s by Southwest Research Institute, the Centro Sviluppo Materiali, and the Societa Nazionale Metanodatti.[4,11] They developed a valid computer model including structural, fluid, and fracture behaviors through more comprehensive and basic approaches, which can better describe and predict the ductile fracture process. In this model, a $CTOA_{max}$ was calculated as a crack driving force in a structure or a fluid of pipelines and was compared with a measured critical CTOA to obtain the reliable and predictable results on characteristics of dynamic ductile fracture propagation and arrest. Here, as a way to indirectly measure the $CTOA_{sc}$, the two-specimen CTOA test (TSCT) method was developed using two modified DWTT specimens having different ligaments under a few fundamental assumptions.[12] Since most of the theoretical works to obtain the $CTOA_{max}$ were conducted in the beginning by two-dimensional analyses, they did not properly consider constraint effects, crack tunneling, or fracture process. More recently, extensive studies have been undertaken to measure the theoretical $CTOA_{max}$ using three-dimensional analyses in consideration of the specimen thickness and to investigate its effects.[9,13,14]

In this study, the relationship between the CVN and DWTT properties of high-toughness (CVN USE $\geq$ 300 J) API X70 pipeline steels was investigated, and the $CTOA_{sc}$ results measured by the TSCT method were correlated with those of the CVN test and DWTT. Also, effects of inverse fracture and separations occurring during the TSCT on the $CTOA_{sc}$ were investigated.

II. EXPERIMENTAL

A. *Materials*

An API X70 grade steel with a yield strength level of 483 MPa (70 ksi) was used in the present study, and its chemical composition was Fe-0.05C-0.27Si-1.24Mn-0.5(Cu + Ni + Mo)-0.1(Nb + V + Ti) (wt pct). Six steel materials were fabricated by varying rolling conditions, as shown in Table I. Rolling was finished at two temperatures, which were the temperature of austenite single-phase region over Ar_3 and the temperature of (austenite + ferrite) two-phase region below Ar_3. After the finish rolling, the steel materials were cooled down acceleratedly to finish cooling temperature (FCT) of about 400 °C, 500 °C, and 600 °C. For convenience, the materials that were rolled in the single-phase region and cooled at different finish cooling temperatures of 400 °C, 500 °C, and 600 °C are referred to as "S4," "S5," and "S6" materials, respectively, while those rolled in the two-phase region and cooled at different finish cooling temperatures of 400 °C, 500 °C, and 600 °C are referred to as "T4," "T5," and "T6" materials, respectively (Table I). The longitudinal-short transverse plane of rolled materials was polished, etched by a 2 pct nital solution, and observed using an optical microscope.

B. *Tensile and Charpy Impact Tests*

Tensile round specimens with a gage diameter of 6 mm and a gage length of 30 mm were prepared in the transverse direction and were tested at room temperature at a crosshead speed of 5 mm/min using a 10-ton Instron machine. Charpy impact tests were performed, using a Tinius Olsen impact tester of 500 J capacity, on subsize CVN specimens with a size of 7.5 × 10 × 55-mm and a transverse-longitudinal (T-L) orientation in the temperature range from −196 °C to 20 °C. In order to reduce errors in the data interpretation, the regression analysis for absorbed impact energy *vs* test temperature was conducted by a hyperbolic tangent curve-fitting method.[15] Based on these analysis data, the energy transition temperature (ETT), which corresponds to the average value of USE and lower shelf energy, was determined. The fracture appearance transition temperature (FATT) at which the area fractions of the cleavage and ductile shear fracture modes were 50 pct was also determined from the observation of fractured CVN specimens.

C. *Drop-Weight Tear Tests*

Drop-weight tear test specimens with a size of 76.2 × 305 × 20 mm in T-L direction were prepared in accordance with the API RP 5L3 specifications,[2] and then a pressed notch was introduced into them. These specimens were tested in the temperature range from −80 °C to 20 °C using an instrumented DWTT testing machine (Model DWTT-100, Imatek, United Kingdom) with a maximum energy capacity of 100,000 J. Fracture initiation and propagation energies were obtained from load-displacement curves using an instrumented system. Here, the fracture propagation energy was evaluated to be the postpeak energy.[16]

The regression analysis for absorbed energy *vs* test temperature was also conducted by a hyperbolic tangent curve fitting method, as in the case of the Charpy impact test.[15] The ETT, USE, and FATT were determined from this analysis. The 85 pct shear appearance transition temperature (85 pct SATT) at which the area fraction of the shear fracture was 85 pct was also determined from the observation of fractured specimens.

D. *Two-Specimen CTOA Tests*

Methods to measure the CTOA include direct measuring, which uses a high-speed camera (over 10,000 frame/s),[9,11] and indirect measuring, which uses J-R curves or TSCT.[12,13,14] The TSCT method, the well-known indirect method, was used in the present study.[12] The pipeline steel materials were machined in the same direction and size to the DWTT specimen, and then two specimens having different ligament, $CTOA_s$ (CTOA shallow) and $CTOA_d$ (CTOA deep) whose notch depth was 10 and 38 mm, respectively, were prepared and tested at −20 °C and 20 °C (room temperature). Figure 1 presents the shape and detailed dimensions of the TSCT specimen.

As illustrated in Figure 2(a), The total energy absorbed during the TSCT can be divided into initiation energy and propagation energy under a few assumptions.[16] Through the comparative analysis of the CTOA approach and the two-parameter approach[17,18] based on extensive experiments, the relationship between S_c in Figure 2(b)[16] and CTOA was identified as

$$S_c = 2\frac{A^*\sigma_0}{(CTOA)_{sc}^{n^*}}$$

Table I. Rolling Conditions and Tensile Properties of the API X70 Steel Materials

Material	Reheat Temp. (°C)	Start Rolling Temp. (°C)	Finish Rolling Temp. (°C)	Start Cooling Temp. (°C)	Finish Cooling Temp. (°C)	Tensile Properties			
						YS (MPa)	TS (MPa)	El (Pct)	YR (Pct)
S4	1200	980	above Ar_3	above Ar_3	410 to 420	500	605	33.8	82.6
S5					490 to 530	506	611	33.4	82.8
S6					590 to 610	504	604	32.9	83.4
T4	1200	910	below Ar_3	below Ar_3	370 to 380	533	655	27.6	81.4
T5					500 to 530	554	612	28.8	90.5
T6					600 to 630	550	615	29.3	89.4

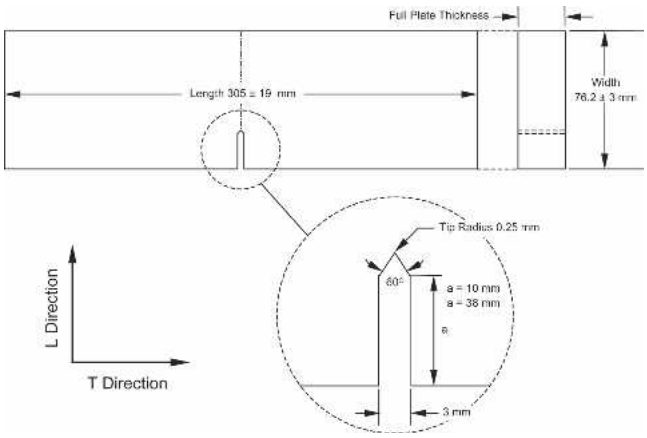

Fig. 1—Shape and dimensions of the specimen used for the TSCT.

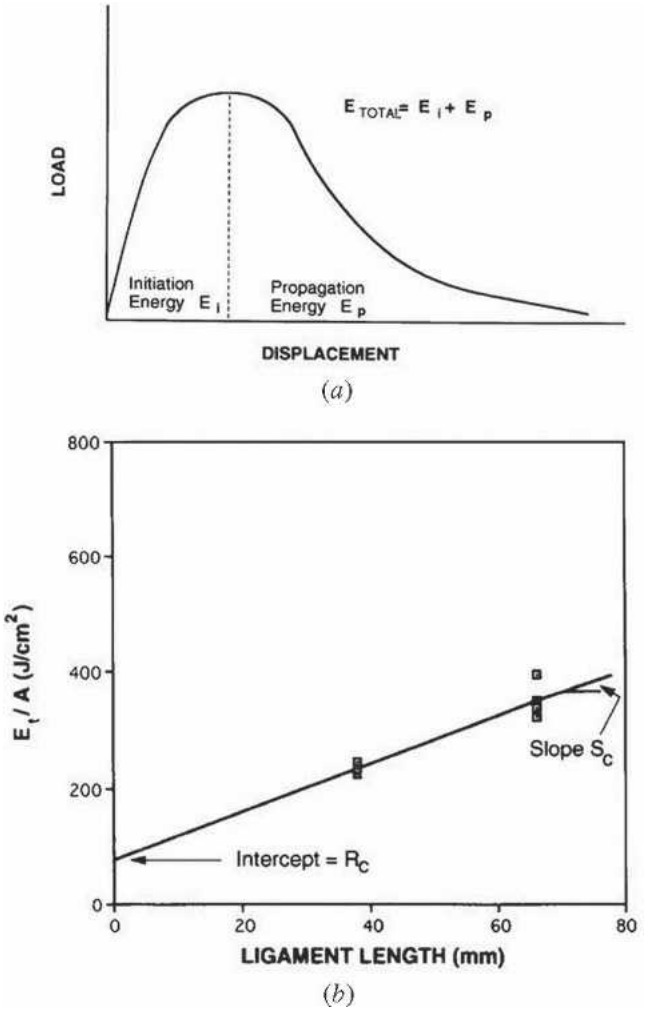

Fig. 2—(*a*) Illustration of initiation energy (E_i) and propagation energy (E_P) obtained from a load-displacement curve and (*b*) relationship between energy density and ligament length to calculate $CTOA_c$.[16]

Here, A^* and r^* are nondimensional constants dependent on the specimen shape and external load, and are found to be 0.35 and 0.45, respectively, in the three-point bending test, while σ_o is flow stress of the material.[19] The R_c (J/mm^2) obtained from the TSCT indicates the energy per unit area required for the formation of two new surfaces, and S_c (J/mm^3) is the energy per unit volume needed for the plastic deformation near the fracture surface.

The procedures of the TSCT[12] can be summarized as follows: (1) preparation of more than three specimens having different ligaments in order to reduce the standard deviation of the $CTOA_{sc}$; (2) conduction of impact tests using an instrumented DWTT tester to obtain total absorbed energy from load-displacement curves; (3) obtaining S_c by linear fitting, as shown in Figure 2(b), after getting absorbed energy per unit area; and (4) substitution of S_c to the following equation:

$$CTOA_{sc} = (180/\pi) C_1 S_c/\sigma_{df}$$

where

C_1 = 2571 in SI units (E/A in J/mm and sdf in N/mm^2);

$S_c = [(E/A)_{shallow} - (E/A)_{deep}]/28$, in J/mm^3

(*cf*. the value 28 is the depth difference between deep and shallow notches);

$(E/A)_{shallow}$ = energy/area for $CTOA_s$ specimen (notch depth = 10 mm);

$(E/A)_{deep}$ = energy/area for $CTOA_d$ specimen (notch depth = 38 mm);

σ_{df} = dynamic flow strength, $0.65(\sigma_{sy} + \sigma_{su})$ (N/mm^2);

σ_{sy} = static yield strength, N/mm^2; and

σ_{su} = static ultimate strength, N/mm^2.

III. RESULTS

A. *Microstructure*

Figure 3(a) through (f) shows optical micrographs of the materials rolled in the single- and two-phase regions. The materials rolled in the single-phase region are mostly composed of acicular ferrite and polygonal ferrite (Figures 3(a) through (c)) and hardly show microstructural variations with FCT. The S6 material shows slightly coarsened ferrite microstructures as some ferrite grains were grown. In the materials rolled in the two-phase region, the volume fraction of polygonal ferrite transformed before or during finish rolling exceeds 85 pct (Figures 3(d) through (f)), and the other phases transformed from retained austenite during or after cooling vary with the FCT. Five to eight volume percent of martensite is present in the T4 material, while some cementite carbides are formed in the T5 and T6 materials.

B. *Tensile Properties*

Room-temperature tensile test results of the materials rolled in the single- and two-phase regions are shown in Table I. All the materials show yield strengths over 483 MPa (70 ksi), satisfying the strength requirement of API X70 grade pipeline steels.[2] The S4 through S6 materials show lower yield and tensile strengths and higher elongation by about 3 pct compared to T4 through T6 materials, and their yield ratios (yield ratio = σ_y/σ_{uts}) are low (below 85 pct). Since the S4 through S6 materials have similar microstructures, they show little changes in tensile properties with the FCT. In the materials rolled in the two-phase region, the T4 material has higher tensile strength and lower yield strength than the T5 and T6 materials and shows lower yield ratio. The T5 and T6 materials

show high yield ratios of about 90 pct, which are considerably higher than that of the T4 material.

C. *Charpy Impact Properties*

The results of USE, FATT, and ETT obtained from the Charpy impact test are summarized in Table II. The S4 through S6 materials show excellent Charpy impact properties because they have lower ETT and higher USE than the T4 through T6 materials. The Charpy properties of the S4 through S6 materials do not show much difference because of little microstructural variation with the FCT. The T4 material containing a considerable amount of martensite shows much lower USE than the T5 and T6 materials, but does not differ much in the transition temperatures of ETT or FATT. The S5 and T5 materials show the best CVN properties among the materials rolled in the single- and two-phase regions, respectively.

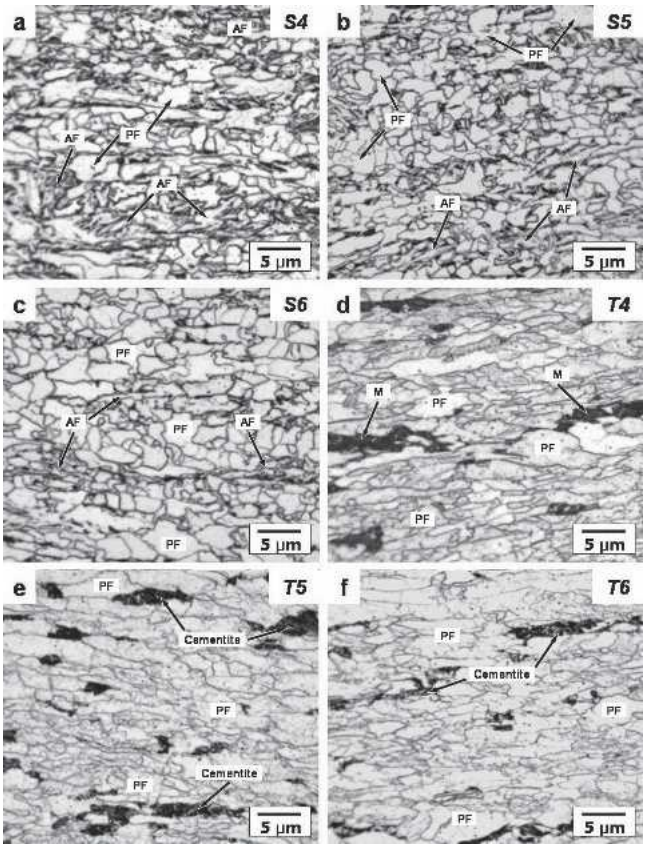

Fig. 3—Optical micrographs of the (*a*) S4, (*b*) S5, (*c*) S6, (*d*) T4, (*e*) T5, and (*f*) T6 materials. Nital etched.

D. *DWTT Properties*

Drop-weight tear test total absorbed energy and pct shear area (pct SA) as a function of test temperature are shown in Figures 4(a) through (d), and the results of USE and 85 pct SATT are summarized in Table II. The S4 through S6 materials show higher absorbed energy in the ductile fracture region above −20 °C than the T4 through T6 materials, and the transition occurs at lower temperatures. In the materials rolled in the single-phase region, except the S6 material, the absorbed energy is very high above 15,000 J at temperatures above −40 °C and abruptly drops at approximately −50 °C to −40 °C (Figure 4(a)). Since the microstructure varies considerably in the T4 through T6 materials, the DWTT energy of the T4 through T6 materials shows larger variance in the ductile fracture region than that of the S4 through S6 materials, and the energy reduction according to the temperature decrease is relatively mild because of the occurrence of separations (Figure 4(b)). In terms of DWTT pct SA, both types of the materials show 100 pct SA at 0 °C or higher, and their 85 pct SATT is mostly −20 °C or lower (Figures 4(c) and (d)), showing excellent DWTT properties. Overall, the S4 through S6 materials show lower FATT and 85 pct SATT than the T4 through T6 materials.

E. *CTOA Properties*

Figure 5(a) and (b) shows DWTT load-displacement curves of the $CTOA_s$ and $CTOA_d$ specimens for the S5 and T5 materials. The load-displacement curves of both the $CTOA_s$ and $CTOA_d$ specimens show almost no deviation, and the maximum load of the $CTOA_s$ specimen is higher than that of the $CTOA_d$ specimen. Though the maximum load of the $CTOA_s$ and $CTOA_d$ specimens of the S5 material does not differ from that of the T5 material, the S5 material shows higher displacement at the maximum load point than the T5 material, and the load reduction after the maximum load point is smoother.

Absorbed energy per unit area as a function of the specimen ligament and linear fitting results, R_c and S_c, are shown in Figure 6(a) through (d), from which the $CTOA_{sc}$ was calculated as listed in Table III. All the plots show the best fitting lines because the data of each ligament do not show much deviation. Comparison of each material's $CTOA_{sc}$ tested at −20 °C and 20 °C (Table III) indicates that the $CTOA_{sc}$ tested at 20 °C is higher than that tested at −20 °C. This seems to be associated with the influence of fracture mode on the

Table II. CVN Impact and DWTT Properties of the API X70 Steel Materials

	CVN Properties			DWTT Properties			
				USE (kJ)			
Material	USE (J)	FATT (°C)	ETT (°C)	Initiation	Propagation	Total	85 Pct SATT (°C)
S4	332	−142	−133	9.4	10.9	20.4	−28
S5	337	−144	−140	9.0	12.6	21.7	−38
S6	329	−134	−131	8.7	10.4	19.1	−42
T4	205	−101	−91	5.2	7.6	12.8	−21
T5	302	−105	−86	8.0	9.0	17.0	−30
T6	285	−99	−84	7.9	8.4	16.3	−20

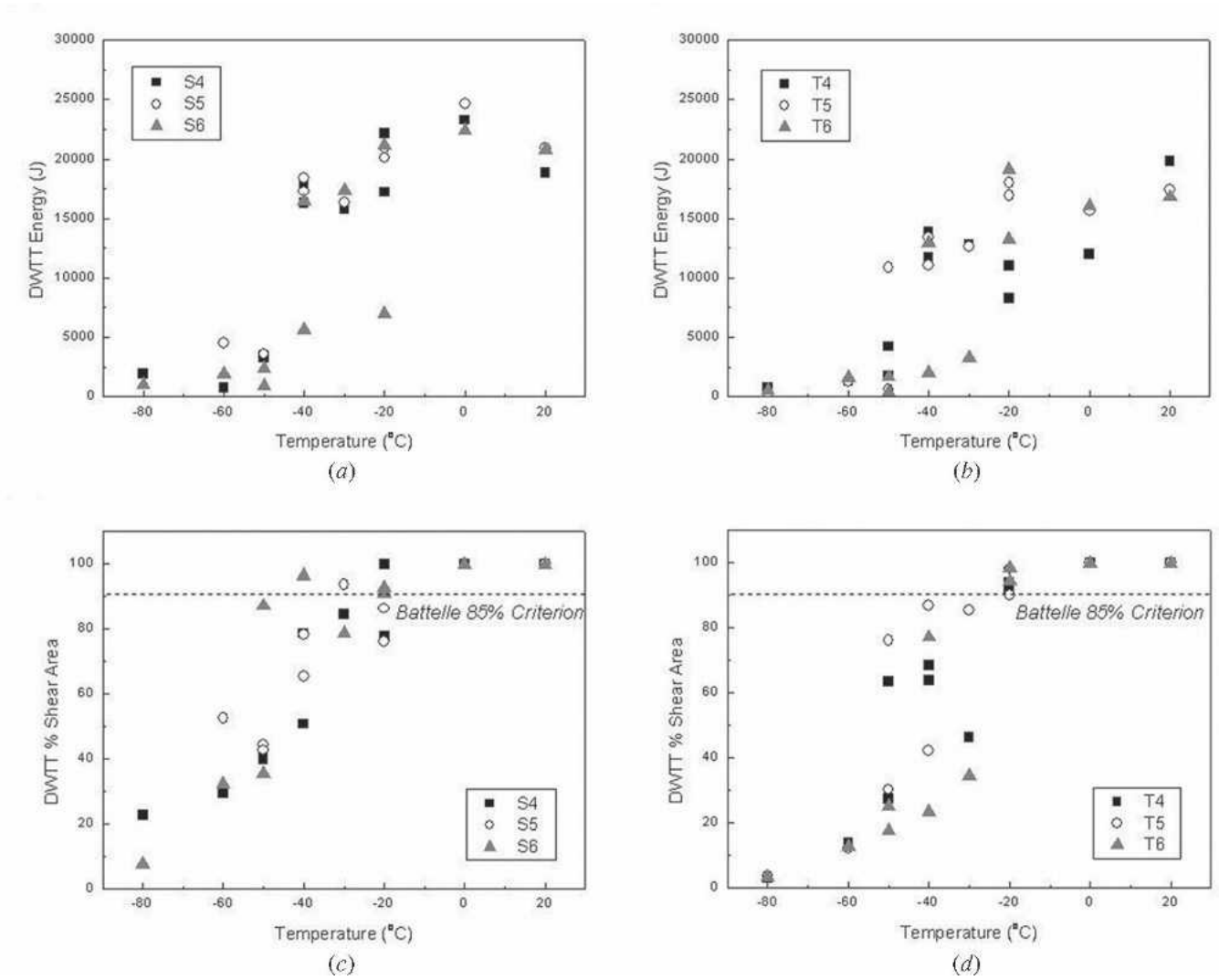

Fig. 4—(*a*) and (*b*) DWTT energy and (*c*) and (*d*) DWTT pct shear area *vs* test temperature for the materials rolled in the (*a*) and (*c*) single- and (*b*) and (*d*) two-phase regions.

$CTOA_{sc}$. Generally speaking, the $CTOA_{sc}$ obtained from the TSCT is valid only when the fracture surface of the $CTOA_s$ and $CTOA_d$ specimens is totally composed of ductile fracture.[12] Observation of the fracture surface of the $CTOA_s$ and $CTOA_d$ specimens reveals that the specimens tested at −20 °C do not show fully ductile fracture as inverse fracture and separations occur in some parts of the fracture surface, whereas the specimens tested at 20 °C shows totally ductile fracture. Consequently, the $CTOA_{sc}$ obtained at −20 °C cannot be valid. Even though the two-test temperatures (−20 °C and 20 °C) belong to the ductile region of the DWTT energy and pct SA curves (Figures 4(a) through (d)) in all the rolled steel materials, considerable attention is required to the fracture mode of the specimens in order to obtain the valid $CTOA_{sc}$ at temperatures near the DWTT transition temperature.

The $CTOA_{sc}$ largely depends on the S_c obtained from the TSCT fitting curve when dynamic flow stress does not differ much. As shown in Table III, the $CTOA_{sc}$ values of the S4 through S6 materials tested at 20 °C are over 20 deg, which are higher than those of the T4 through T6 materials. The materials rolled in the two-phase region, except the T4 material, show relatively high $CTOA_{sc}$ values over 14 deg. According to a recent study of high-toughness materials, the $CTOA_{sc}$ measured from the TSCT appears to be higher than the $CTOA_{sc}$ directly measured by a high-speed camera.[11]

IV. DISCUSSION

A comprehensive, comparative analysis of the CVN, DWTT, and CTOA data of various pipeline steels currently available in the literature was made in this discussion section. The known relationships between CVN and DWTT energy density were confirmed in pipeline steels with a wide toughness range, and the correlations between them and CTOA were investigated. After dividing DWTT total energy density into initiation and propagation energy density, correlations befitting for each property were studied.

A. *Relationships between CVN and DWTT Energy Density*

After energy density is defined as energy per unit area (unit: J/mm^2), Figure 7(a) shows the CVN and DWTT total energy density of various pipeline steels currently produced and the known relationships between them. Since the CVN and DWTT energy density of the pipeline steel materials

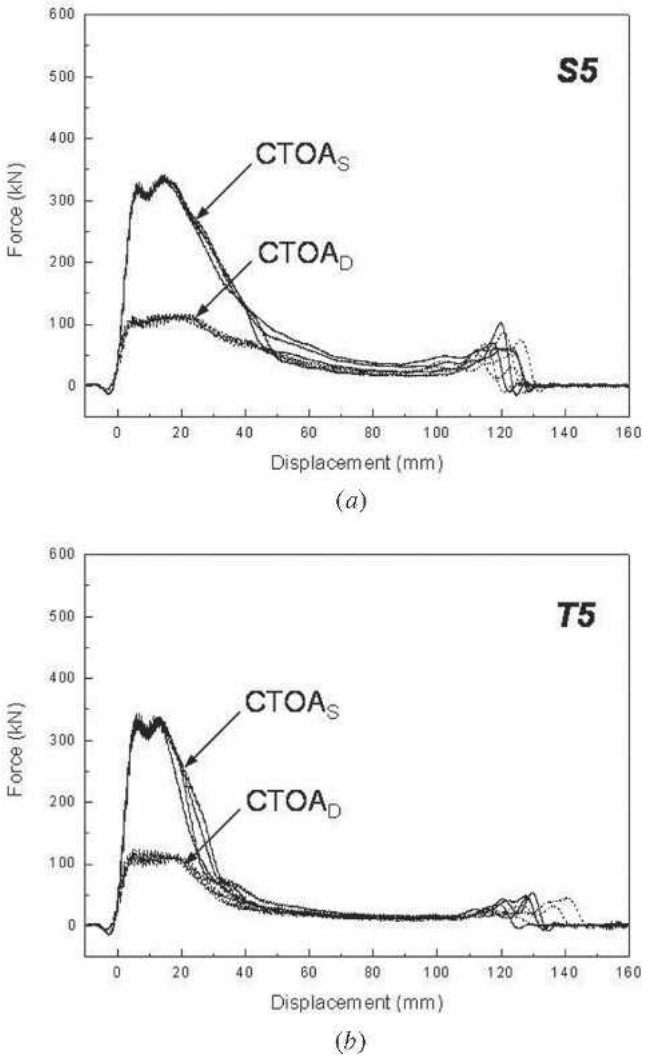

Fig. 5—Load-displacement curves of the (*a*) $CTOA_s$ and (*b*) $CTOA_d$ specimens for the S5 and T5 materials.

fabricated in the present study is much higher than that of other steels, all the present pipeline steel materials can be considered as very-high-toughness steels. Most data are slightly off the known relationships, such as $(E/A)_{DWTT} = 3(E/A)_{CVN} + 0.63$ (J/mm^2) and $(E/A)_{DWTT} = 1.9(E/A)_{CVN} + 1.57$ (J/mm^2).[2,10,16–25] This is because a rising shelf phenomenon or separations readily occur in currently fabricated high-toughness steels during the CVN or DWTT impact tests, and thus the effects of initiation or propagation energy on DWTT total energy vary. According to an actual testing of a high-strength X100 pipeline steel (YS $\geq$ 690 MPa) by the Centro Sviluppo Materiali,[18] the DWTT energy density corresponding to the CVN energy density varied with the specimen thickness and differed from other grade pipeline steels (X60 through X80 grade).[14,16,22] In addition, many data are observed to be placed below the Battelle relationship adopted by API. This indicates that the DWTT energy, including higher propagation energy, do not increase much in high-toughness steels, whereas the CVN energy considerably increases in comparison with earlier, conventional steels. In conventional, low-toughness steels with low absorbed energy, the CVN and DWTT total energy densities well satisfy a linear relationship, but it fits in a roughly linear relationship within a wide range of scatters in currently produced high-toughness steels.[23,24] Therefore, errors can be committed when predicting the arrest toughness of actual pipeline steels because linear relationships between CVN and DWTT properties cannot be accurately consistent by various factors as the toughness increases.

Figure 7(b) illustrates the variations in DWTT total, initiation, and propagation energy density, together with the latest Centro Sviluppo Materiali data,[25] as a function of CVN total energy density. According to the fitting results between CVN total energy density and DWTT initiation energy density, they surprisingly show an almost 1:1 linear correlation. This indicates that the CVN total energy density is more consistent with the DWTT initiation energy density than the DWTT total or propagation energy density because most of the CVN energy of high-toughness steels is related with the fracture initiation energy at the notch due to the short fracture path in the case of the CVN specimen. It is thus desirable to use the DWTT initiation energy instead of DWTT total energy in order to more properly apply the correlation between CVN and DWTT energy density. At the CVN total energy density of 3 to 5 J/mm^2, the DWTT total energy density shows an almost linear relation with the CVN total energy density and then greatly increases at the CVN total energy density above 5 J/mm^2. This is because the DWTT initiation energy density increases steadily in proportion to the CVN total energy density, but the DWTT propagation energy density substantially increases in the range of the higher CVN total energy density. Thus, the DWTT propagation energy density affects the DWTT total energy density to a greater extent.

B. *Relationships between CTOA, CVN, and DWTT Properties*

Figure 8(a) and (b) show the correlations of CTOA with CVN and DWTT total energy density, respectively. Because the CVN total energy density generally increases as the CTOA increases, there is a good linear correlation between them. Ogasawara[26] reported in the mid 1980s that the CTOA was linearly related with the CVN total energy in low-strength, low-toughness pipeline steels having various alloy compositions and microstructures (Figure 8(a)). This implies that the CVN total energy well indicated the resistance to dynamic ductile fracture of low-toughness pipeline steels, which is reasonably evaluated by the CTOA. Other data[18,25] having total energy density below 4 J/mm^2, except the test results by O'Donoghue *et al.*,[16] are roughly in a linear relation with the CTOA, although they show some scattering. However, the very-high-toughness pipeline steel materials, having high CVN total energy density over 4 J/mm^2 fabricated in the present study, tend to show minor increase in CVN energy density *vs* CTOA (Figure 8(a)). Because currently produced very-high-toughness steels include much more initiation energy than typical high-toughness steels, not only does the CVN energy density not properly represent the dynamic ductile fracture resistance of high-toughness pipeline steels, but it also does not show any proper relation with the CTOA, which is related with the propagation speed of ductile crack.[11]

Like the CVN total energy density, the DWTT total energy density is also in a linear relation with the CTOA (Figure 8(b)).

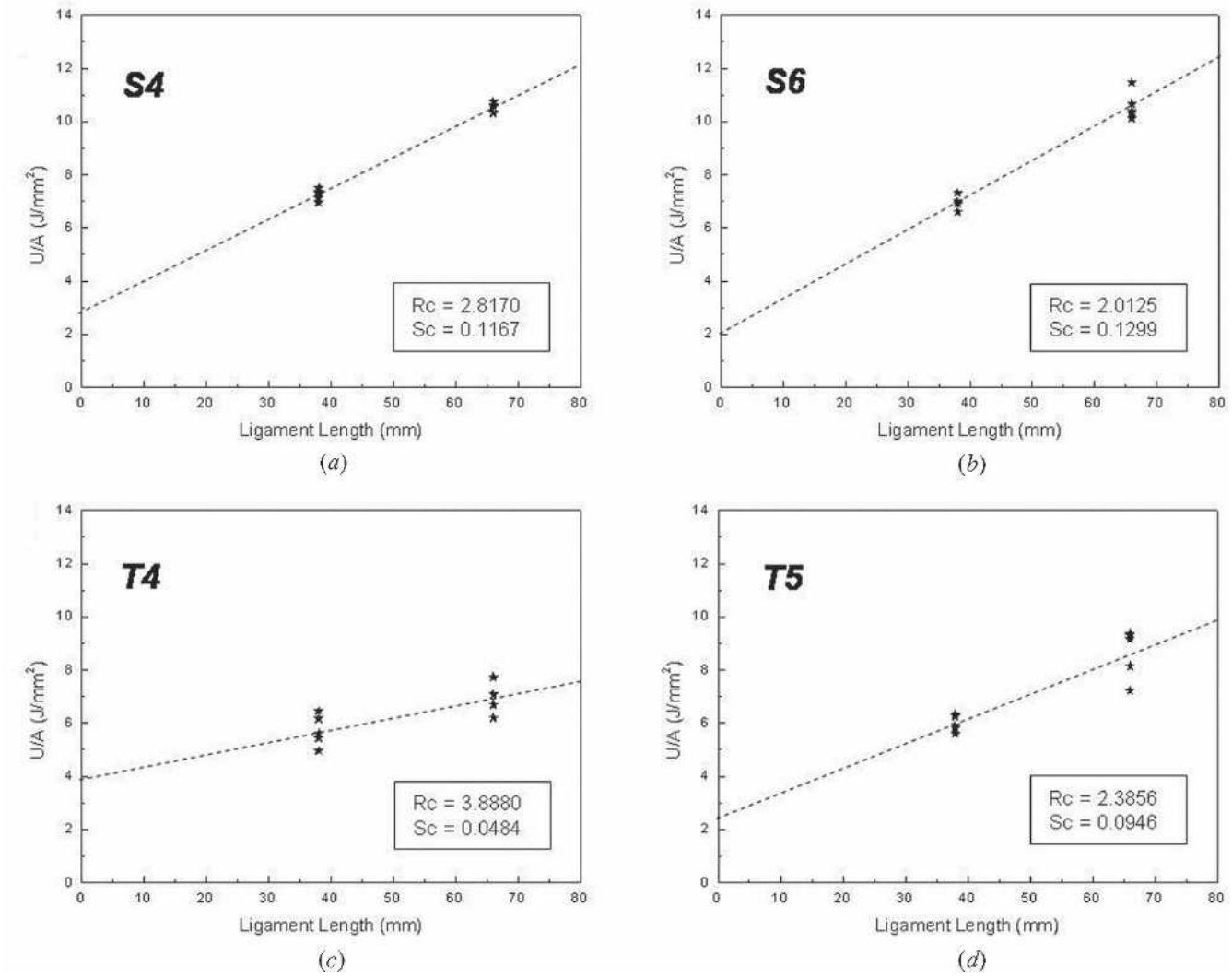

Fig. 6—Absorbed energy density as a function of ligament length for the (*a*) S4, (*b*) S6, (*c*) T4, and (*d*) T5 materials.

Table III. CTOA Test Results Obtained from the TSCT Method

Material	Test Temp. (°C)	Fracture Mode	σ_{oD} (N/mm^2)	R_c (J/mm^2)	S_c (J/mm^3)	CTOA$_{sc}$ (^{O})	sin (2CTOA$_{sc}$)
S4	20 (room temp.)	fully ductile	718.17	2.8170	0.1167	23.9	0.742
S5			726.39	—*	—*	—*	—*
S6			719.74	2.0125	0.1299	26.6	0.800
T4			772.17	3.8880	0.0484	9.2	0.317
T5			757.63	2.3856	0.0946	18.4	0.599
T6			756.95	2.8140	0.0718	14.0	0.469
S4	−20	ductile fracture with a small amount of inverse fracture and separation	718.17	3.5112	0.0899	18.4	—
S5			726.39	3.9123	0.0790	16.0	—
S6			719.74	2.6072	0.0749	15.3	—
T4			772.17	1.6767	0.0686	13.1	—
T5			757.63	3.4783	0.0464	9.0	—
T6			756.95	3.2507	0.0513	10.0	—

*Not tested.

However, the DWTT total energy density *vs* CTOA shows more scattering overall than the CVN total energy *vs* CTOA. Searching for a formula representing the relationship between DWTT energy density and CTOA reveals that the value of sin (2CTOA) is relatively well in proportion to the DWTT propagation energy density (Figure 9(a)). In particular, the

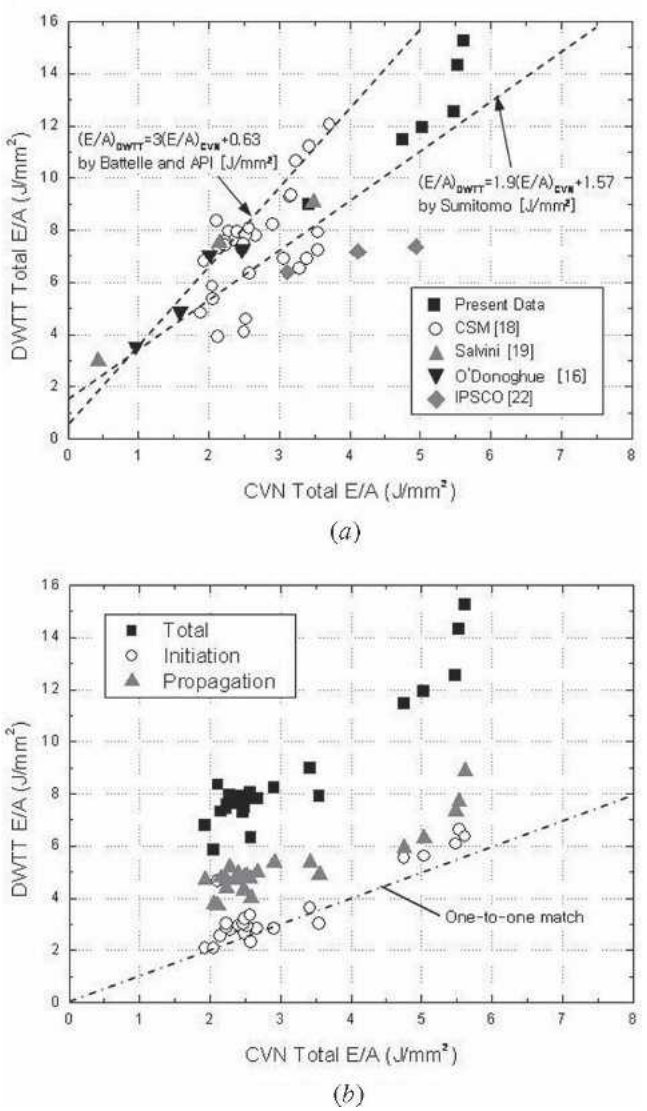

Fig. 7—Relationships (*a*) between CVN total energy density and DWTT total energy density[16,18,19,22] and (*b*) between CVN total energy density and DWTT total, initiation, and propagation energy densities.[25]

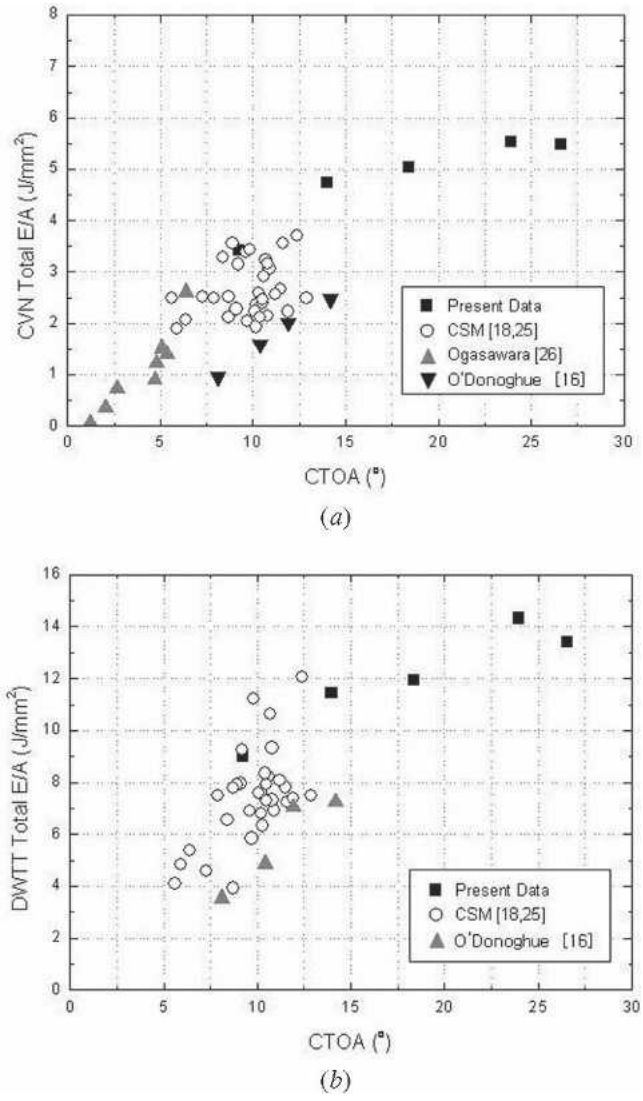

Fig. 8—Relationships between CTOA and (*a*) CVN energy density[16,18,25,26] and (*b*) DWTT total energy density.[16,18,25]

DWTT propagation energy density shows a more reliable linear relationship than the DWTT total energy density (Figure 9(b)). This indicates that the CTOA has good consistency with the propagation energy density absorbed during the fracture process of the DWTT specimen. According to a recent study by Rudland *et al*.,[11] in which the CTOA was directly measured during the fracture process of the DWTT specimen, the propagation energy of the DWTT specimen at a steady state having a certain CTOA with the crack growth was reduced steadily, and the crack propagation speed was constant. As this steady reduction of the DWTT propagation energy is found to be unrelated with the notch type of the DWTT specimen, searching for empirical relationships between DWTT energy and CTOA seems possible. Inducing correlations between the two variables may not prove to be useful because specific relationships between the two variables are not clearly reached due to inherent differences between them and because serious scattering may exist. Despite the presence of deviation to a certain extent in inducing these relationships, they do have an advantage enabling approximate prediction of the CTOA in pipeline steels. In order to find more reliable relationships between these two variables, more extensive studies to investigate the effects of various factors such as materials, specimen shape, and testing method on DWTT or CTOA properties will be required.[27]

Figure 10(a) and (b) shows all the values of CVN and DWTT absorbed energy density, transition temperature, and CTOA of the materials rolled in the single- and two-phase regions. The S4 through S6 materials show lower transition temperature of the CVN ETT or DWTT 85 pct SATT, higher absorbed energy density of CVN USE and DWTT USE, and larger CTOA, indicating comparatively better fracture properties than the T4 through T6 materials. In particular, the S5 and T5 materials fabricated at the FCT of 500 °C show the best fracture properties in each type of materials. In the materials rolled in the two-phase region, the T4 material shows worst fracture properties overall because the absorbed energy density and CTOA decrease due to partial formation of martensite, although its transition temperature is not much different from that of the other materials. These findings indicate that the steel materials rolled in the single-phase region, properly

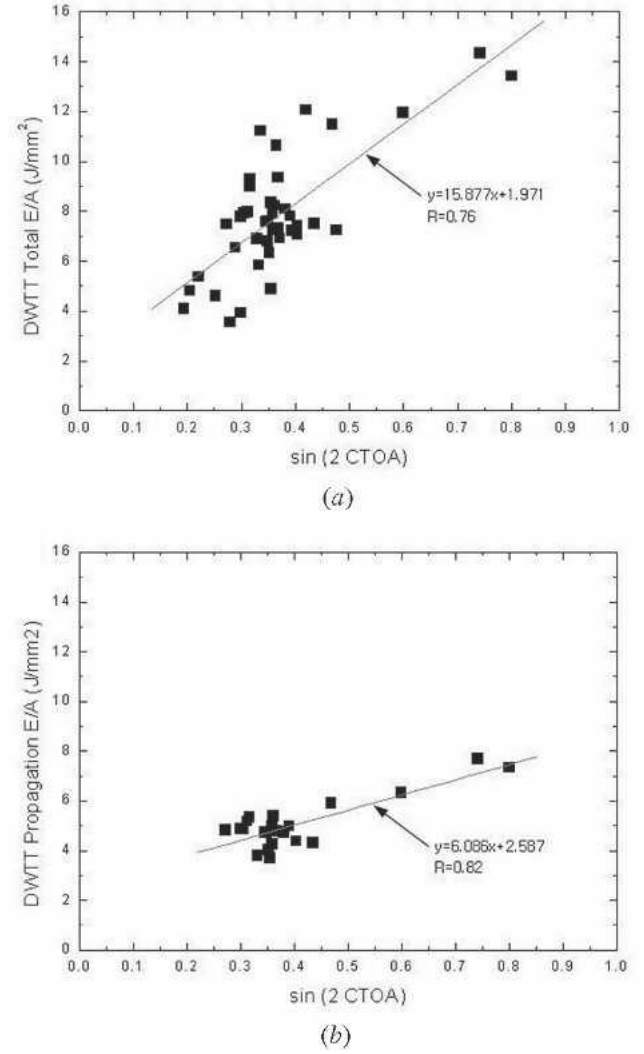

Fig. 9—Relationship between sin (2CTOA) and (*a*) DWTT total energy density[16,18,25] and (*b*) DWTT propagation energy density.[25]

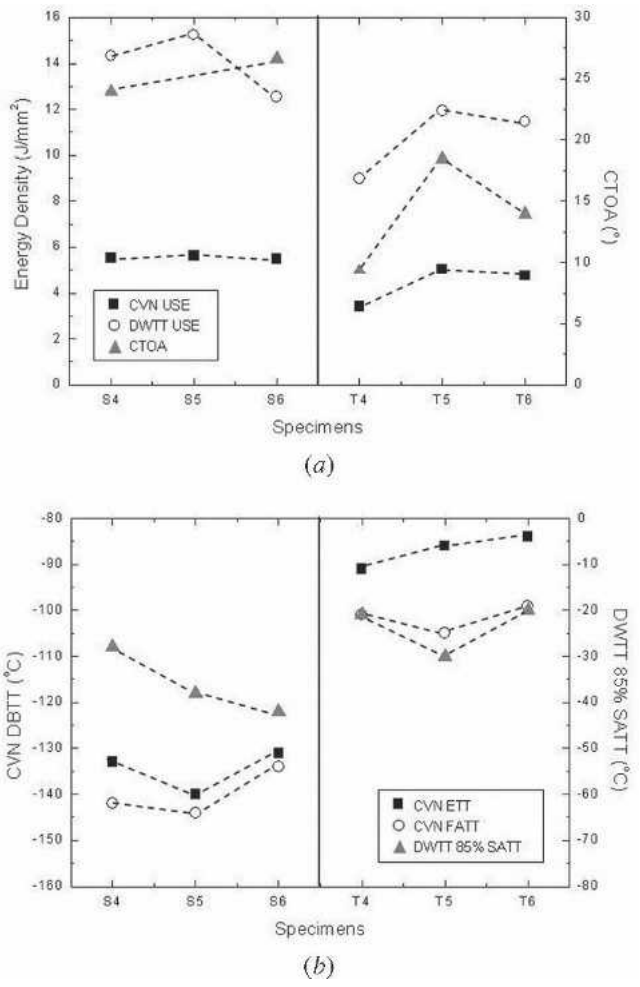

Fig. 10—(*a*) DWTT USE obtained from DWTT, CVN USE obtained from CVN test, and CTOA obtained from TSCT, and (*b*) DWTT 85 pct SATT obtained from DWTT and CVN ETT and FATT obtained from CVN test for all the materials used in this study.

composed of acicular ferrite and fine polygonal ferrite, are appropriate for high-toughness pipeline steels because they have more excellent tensile and fracture properties.

Active studies on the CTOA have been undertaken recently, but it has not settled yet as a universal evaluation method because of its complicated and difficult measuring techniques. Moreover, further studies are required for finding relationships between CTOA, CVN, and DWTT properties. Thus, the present study signifies a good start by investigating the correlations of the known CVN and DWTT energy density for various high-toughness pipeline steels and by elucidating the relationship of the CTOA with them. To develop more reliable and universal testing methods to evaluate fracture properties of pipeline steels, clearer understanding and more sufficient verification of the problems inherently existing in evaluation methods and the relationship between them are needed.

V. CONCLUSIONS

In this study, CVN, DWTT, and CTOA properties of high-toughness pipeline steels were evaluated, and the relationships between them were investigated to reach following conclusions.

1. When the test temperature during the CTOA measurement of high-toughness pipeline steels by the TSCT method was close to the transition temperature even in the ductile fracture region, separations or inverse fracture occurred on the fracture surface of the $CTOA_s$ and $CTOA_d$ specimens. Thus, the measured CTOA showed a considerable difference from the actual one at room temperature.
2. The DWTT total energy density of high-toughness pipeline steels showed a roughly proportional relationship with the CVN total energy density within the wide range of scattering. After dividing the DWTT total energy density into the initiation and propagation energy density, the relationships with the CVN total energy density were investigated. According to the analysis data, the DWTT initiation density was in an almost 1:1 linear relationship with the CVN total energy density.
3. The CTOA had a better correlation with the DWTT propagation energy density or the CVN total energy density than with the DWTT total energy density. In particular, the value of sin (2CTOA) reliably represented a linearly proportional relation with the propagation energy density.

4. The materials rolled in the single-phase region showed lower transition temperature of the CVN ETT or DWTT 85 pct SATT, higher absorbed energy density of CVN USE and DWTT USE, and larger CTOA, indicating better fracture properties than those rolled in the two-phase region. The S5 and T5 materials fabricated at the FCT of 500 °C showed the best fracture properties in each type of materials.

ACKNOWLEDGMENTS

This work was financially supported by the National Research Laboratory Program, funded by the Korea Science and Engineering Foundation and by POSCO, under Contract No. PL-03909. The authors thank Drs. Jang Yong Yoo, Seong Soo Ahn, and Dong Han Suh, POSCO, for their help with the DWTT testing and data analyses.

REFERENCES

1. R.J. Eiber, T.A. Bubenik, and W.A. Maxey: *Fracture Control Technology for Natural Gas Pipelines*, Pipeline Research Council International Inc., 1993.
2. *API Recommended Practice 5L3*, American Petroleum Institute, 1996.
3. G.M. Wilkowski, W.A. Maxey, and R.J. Eiber: *Proc. Symp. on What Does Charpy Test Really Tell Us?*, ASM, Metals Park, OH, 1978, pp. 201-26.
4. R. Denys: *Pipeline Technology*, Elsevier, Amsterdam, 2000, vols. I and II.
5. D.J. Horsley: *Eng. Fract. Mech*., 2003, vol. 70, pp. 547-52.
6. H.N. Han, C.-S. Oh, D.W. Suh, C.G. Lee, T.-H. Lee, and S.-J. Kim: *Met. Mater. Int*., 2004, vol. 10, pp. 221-29.
7. J.C. Newman, Jr.: *ASTM STP*, 1984, vol. 833, pp. 93-117.
8. T.-H. Lee, C.-S. Oh, C.G. Lee, S.-J. Kim, and S. Takaki: *Met. Mater. Int*., 2004, vol. 10, pp. 231-36.
9. J.C. Newman, Jr., M.A. James, and U. Zerbst: *Eng. Fract. Mech*., 2003, vol. 70, pp. 371-85.
10. A.B. Rothwell: in *Pipeline Technology*, R. Deny, ed., 2000, vol. 1, pp. 387-405.
11. D.L. Rudland, G.M. Wilkowski, Z. Feng, Y.-Y. Wang, D. Horsley, and A. Glover: *Eng. Fract. Mech*., 2003, vol. 70, pp. 567-77.
12. G. Demofonti, G. Buzzichelli, S. Venzi, and M. Kanninen: in *Pipeline Technology*, R. Denys, ed., 1995, vol. 2, pp. 503-12.
13. W.R. Lloyd and F.A. McClintock: *Eng. Fract. Mech*., 2003, vol. 70, pp. 387-415.
14. L.N. Pussegoda, S. Verbit, A. Dinovitzer, W. Tyson, A. Glover, L. Collins, and L. Carlson: *Proc. 2000 Int. Pipeline Conf*., ASME, Philadelphia, PA, 2000, vol. 1, pp. 247-54.
15. W. Oldfield: *ASTM Standardizations News*, 1975, pp. 24-29.
16. P.E. O'Donoghue, M.F. Kanninen, C.P. Leung, G. Demofonti, and S. Venzi: *Int. J. Pressure Vessel Piping*, 1997, vol. 70, pp. 11-25.
17. A.H. Priest and B. Holmes: *Int. J. Fract*., 1981, vol. 17, pp. 277-99.
18. G. Mannucci and D. Harris: *Fracture Properties of API X100 Gas Pipeline Steels*, Final Report, European Commission, 2002.
19. P. Salvini, A. Fonzo, and G. Mannucci: *Eng. Fract. Mech*., 2003, vol. 70, pp. 553-66.
20. G.M. Wilkowski, W.A. Maxey, and R.J. Eiber: *Can. Metall. Q*., 1980, vol. 19, pp. 59-77.
21. L. Pussegoda, L. Malik, A. Dinovitzer, B.A. Graville, and A.B. Rothwell: *Proc. 2000 Int. Pipeline Conf*., J.R. Ellwood, ed., ASME, Philadelphia, PA, 2000, vol. 1, pp. 239-45.
22. L.E. Collins, M. Kostic, T. Lawrence, R. Mackenzie, and N. Townley: *Proc. 2000 Int. Pipeline Conf*., ASME, Philadelphia, PA, 2000, vol. 1, pp. 185-91.
23. B.N. Leis: in *Pipeline Technology*, R. Denys, ed., Elsevier, Amsterdam, 2000, vol. I, pp. 343-58.
24. G. Wilkowski, Y.-Y. Wang, and D. Rudland: in *Pipeline Technology*, R. Denys, ed., Elsevier, Amsterdam, 2000, vol. I, pp. 359-86.
25. G. Demofonti, G. Mannucci, M. Di Biagio, H.G. Hillenbrand, and D. Harris: *Pipeline Technology Conf*., R. Denys, ed., Scientific Surveys, Ltd., Ostend, Belgium, 2004, vol. I, pp. 467-81.
26. M. Ogasawara: *Nippon Steel Tech. Rep*., 1983, vol. 21, pp. 339-45.
27. D.L. Rudland, Y.Y. Wang, G.M. Wilkowski, and D. Horsley: *Eng. Fract. Mech*., 2004, vol. 71, pp. 2533-49.